


Particle-hole asymmetric lifetimes promoted by spin and orbital fluctuations in SrVO₃ monolayers

Matthias Pickem ^{1,*} Jan M. Tomczak ¹ and Karsten Held ¹

¹*Institute for Solid State Physics, TU Wien, Vienna, Austria*

(Dated: January 19, 2022)

The two-dimensional nature of engineered transition-metal ultra-thin oxide films offers a large playground of yet to be fully understood physics. Here, we study pristine SrVO₃ monolayers that have recently been predicted to display a variety of magnetic and orbital orders. Above all ordering temperatures, we find that the associated non-local fluctuations lead to a momentum differentiation in the self-energy, particularly in the scattering rate. In the one-band 2D Hubbard model, momentum-selectivity on the Fermi surface (" $k = k_F$ ") is known to lead to pseudogap physics. Here instead, in the multi-orbital case, we evidence a differentiation between momenta on the occupied (" $k < k_F$ ") and the unoccupied side (" $k > k_F$ ") of the Fermi surface. Our work, based on the dynamical vertex approximation, complements the understanding of spectral signatures of non-local fluctuations, calls to (re)examine other ultra-thin oxide films and interfaces with methods beyond dynamical mean-field theory, and may point to correlation-enhanced thermoelectric effects.

I. INTRODUCTION

In the vicinity of phase transitions and in low-dimensional systems, non-local long-range fluctuations are known to proliferate. These are not only crucial for the critical behavior but may also lead to a strong enhancement of the scattering rate, i.e., a dampening of the quasiparticle lifetime. In three dimensions it is still debated¹⁻³ whether this scattering rate is actually diverging at a phase transition or approaches a large but finite value. Even more peculiar is the situation in two dimensions. There, an actual phase transition—associated with the breaking of continuous symmetries—is prohibited. Nonetheless non-local long-range fluctuation may still become huge and can result in the famous pseudogap that has been experimentally observed in cuprate superconductors⁴⁻⁷. The pseudogap arises from a pronounced momentum differentiation of the scattering rate at low energy. It is largest in the anti-nodal direction where eventually a gap opens at low enough temperatures. One possible explanation are long-range *antiferromagnetic* spin fluctuations⁸⁻¹³, with the momentum differentiation originating from the perfect antiferromagnetic nesting at the hot spots^{1,14-18}, from the vicinity to a van Hove singularity in the anti-nodal direction¹⁹⁻²², or from the spin-fermion vertex turning complex at strong coupling²³. It has also been suggested, on the basis of model studies, that a pseudogap phase can be driven by *ferromagnetic* fluctuations²⁴⁻²⁸. While pseudogap physics is mostly associated with cuprates, it has also been evidenced in other layered materials³⁰: iron pnictides³¹⁻³⁴ and chalcogenides³⁵, (layered) nickelates³⁶, and iridates³⁷. However, the origin of momentum-differentiated scattering rates is far from understood.

Here, we study a material that is two-dimensional by engineering: a monolayer of SrVO₃. In the bulk, SrVO₃ is a correlated paramagnetic metal^{38,39} with a correlation-induced kink^{40,41} linked to the effective

Kondo temperature⁴². Grown as a film, it is known to undergo a metal-insulator transition below a critical thickness when deposited on an SrTiO₃⁴³⁻⁴⁵ or LSAT⁴⁶ substrate. We focus on a monolayer of SrVO₃ grown on the common SrTiO₃ substrate and consider two different terminations of the film to the vacuum: VO₂ and SrO, see insets of Fig. 1. Only the former has been evidenced experimentally⁴⁷, but it could be preferable to cover the films with a SrTiO₃ capping layer which leads to a structure more akin to the SrO termination. Such a capping layer also prevents a surface reconstruction with oxygen adatoms, which result in a dead surface layer⁴⁸, at least for slightly thicker films. A preceding study²⁹, based on dynamical mean-field theory (DMFT)⁴⁹⁻⁵¹, revealed a rich variety of orbital ordered and magnetic phases as a function of doping, see Fig. 1. Experimentally, the phase diagrams could be perused by applying a gate voltage.

In the present paper, we go beyond DMFT and study the effect of non-local fluctuations on spectral properties using the dynamical vertex approximation (DVA)⁵²⁻⁵⁵. As for cuprates, we find that strong long-range fluctuations lead to a substantial momentum-dependence in the self-energy. In stark contrast to the cuprates, however, in ultrathin films of SrVO₃ the momentum differentiation does not distinguish momenta *on* the Fermi surface but those *perpendicular* to it. For example for the SrO-termination and antiferromagnetic spin fluctuations (above the red dome in Fig. 1a), occupied states with momenta below the Fermi surface have a long, Fermi liquid-like lifetime. Instead, unoccupied states above the Fermi surface have short lifetimes and even kinks (downturns) in the self-energy, signaling a depletion of states. For orbital-ordering and ferromagnetic fluctuations (above green and blue regions) it is *vice versa*. The same is true for the VO₂-termination and the most relevant xz/yz orbitals in the regime of orbital and incommensurate magnetic fluctuations above half-filling ($n > 1$ in Fig. 1b, above the green and blue regions). Below half-filling, instead, non-local correlations only have a minor impact

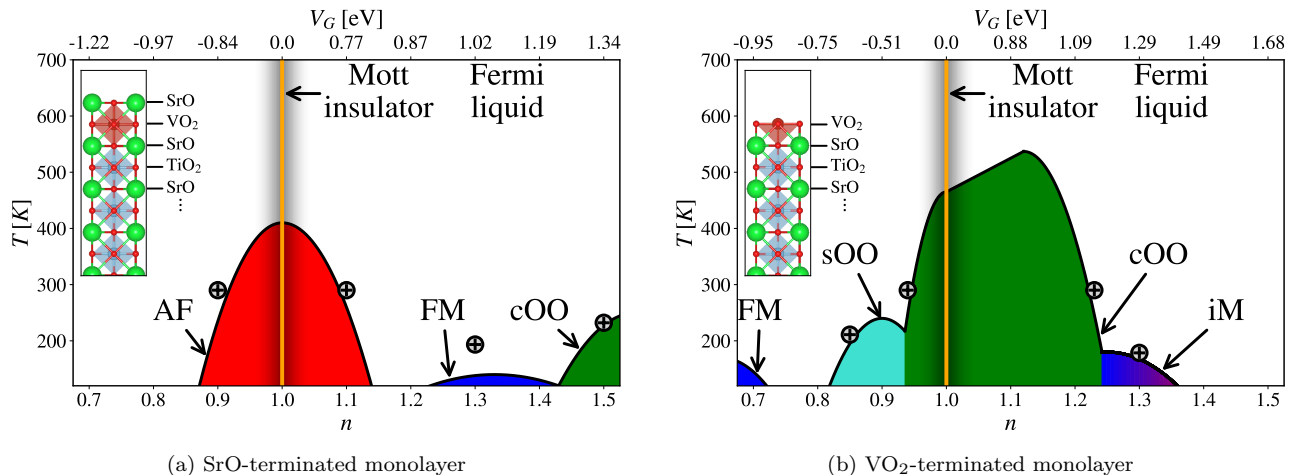


FIG. 1. **Phase diagrams.** (a) SrO- and (b) VO₂-terminated SrVO₃-monolayer on top of a SrTiO₃ substrate (see insets for crystal structures) exhibit numerous phases as a function of electrons per site (n ; lower x -axis) in the low-energy vanadium t_{2g} orbitals or gate voltage (V_G ; upper x -axis): antiferromagnetism (AF: red), ferromagnetism (FM: blue), incommensurate magnetism (iM: blueish), checkerboard orbital order (cOO: green), stripe orbital order (sOO: turquoise). The colored domes mark the occurrence of long-range order within dynamical mean-field theory (DMFT); adapted from Ref. 29. The “+”-marks indicate points for which we present DfA (and DMFT) data in the present paper.

on the self-energy of this termination.

A pronounced particle-hole asymmetry in the *real part* of the self-energy is a common phenomenon, mostly owing to non-local exchange. For example, in *GW* calculations^{56–58} it leads to larger semiconductor band gaps than in density functional theory. For the *imaginary part* of the self-energy (the scattering rate), however, such an asymmetry has, to the best of our knowledge, not been reported so far. The particle-hole asymmetric lifetimes arising here from a momentum-selectivity of renormalizations can complement more ubiquitous orbital-selective asymmetries and could drive large thermoelectric effects.

The outline of the paper is as follows: Section II provides information on the employed electronic structure methods. Section III presents the DMFT Fermi surfaces and spectral functions and the trends upon doping the SrVO₃ monolayer. Non-local fluctuations in AbinitioDfA suppress ordering instabilities but strong long-range fluctuations persist and affect spectra and self-energies. An analysis of the AbinitioDfA results and the evidenced momentum selectivity are presented in Section IV, and further discussed in Section V. Finally, Section VI summarizes our conclusions.

II. METHOD

The crystal structures used are identical to Ref. 29: Density function theory (DFT) calculations are based on the WIEN2K package^{59,60} with PBE⁶¹ as exchange-correlation potential. We construct a slab as displayed in the insets of Fig. 1 consisting of one unit cell of SrVO₃ on top six unit cells of the SrTiO₃ substrate and sur-

rounded (in z -direction) by sufficient vacuum of about 10Å to both sides. While the in-plane lattice constant of the heterostructure is locked to the (theoretical) SrTiO₃ substrate⁶² ($a_{\text{SrTiO}_3}^{\text{PBE}} = 3.95\text{\AA}$) all other internal atomic positions are relaxed, except for the two unit cells of SrTiO₃ furthest away from SrVO₃. The WIEN2K band-structure is then projected onto maximally localized V- t_{2g} Wannier orbitals, using the WIEN2Wannier⁶³ interface to Wannier90⁶⁴. The thus obtained Wannier Hamiltonian is supplemented by a Kanamori interaction using $U = 5\text{eV}$, $J = 0.75\text{eV}$, $U' = 3.5\text{eV}$, and solved by dynamical mean-field theory (DMFT)^{51,65}. Doping is modeled by a posterior-to-DFT adjustment of the chemical potential in DMFT. For DMFT spectral functions, analytic continuation was performed with the maximum entropy method implemented in `ana_cont`^{66,67}. There, the hyper parameter α was determined with the `chi2kink` method and a preblur window size of $\sigma = 0.05\text{eV}$ was employed.

In this paper we go beyond DMFT^{55,68} and treat non-local correlations in the SrVO₃ film with AbinitioDfA^{54,69,70}. Contrary to finite-size cluster methods, the DfA approach^{52,53,55} and other, closely related diagrammatic extensions of DMFT^{55,71–76} are not limited to short-range fluctuations. It well describes pseudogaps induced by antiferromagnetic fluctuations in the one-band 2D Hubbard model^{12,77–83} and (quantum) critical behavior^{2,84–86}. Orbital-ordering and ferromagnetic fluctuations have hitherto not been studied by DfA or other diagrammatic extensions of DMFT. For the AbinitioDfA, we here calculate the local particle-hole irreducible vertex at DMFT self-consistency by continuous-time quantum Monte Carlo simulations in the hybridization expansion^{87,88} using `w2dynamics`⁸⁹

with worm sampling⁹⁰. From this local vertex we subsequently calculate the particle-hole and transversal particle-hole Bethe-Salpeter ladder diagrams, and, through the Schwinger-Dyson equation, the non-local self-energy. This way we include non-local correlation effects in the self-energy. The DGA chemical potential was readjusted to fix the total number of electrons to the considered doping level. In this study we apply DGA in a one-shot setting, forgoing non-local self-consistency⁹¹. For a review of the method, see Ref. 55; for computational details of the AbinitioDGA see Ref. 70. DGA and DMFT Fermi surfaces were obtained from the Green's function at imaginary time $\tau = \beta/2$ ($\beta = 1/k_B T$). This procedure corresponds to a spectral function $A(\mathbf{k}, \omega = 0)$ that is averaged over a frequency-interval $\sim k_B T$ around the Fermi level.

III. DMFT: ORBITAL EFFECTS

The DMFT phase diagram Fig. 1 shows, as a function of doping and surface termination, a rich variety of different magnetic and orbitally ordered phases²⁹. Non-local fluctuations will strongly suppress the DMFT phase transitions in two dimensions but lead, at the same time, to strong scattering rates and self-energy corrections. In Sec. IV, we will study these renormalizations using the DGA at the (n, T) -points indicated in Fig. 1. The temperatures have been chosen so that we are close to the respective phase transitions in DMFT and, thus, can expect pronounced non-local correlations⁹². Before turning to these DGA results, in this Section we first analyze the DMFT Fermi surfaces and \mathbf{k} -integrated spectra at the same fillings (orbitally resolved occupations, DMFT susceptibilities, and \mathbf{k} -integrated DMFT spectra at filling $n = 1$ with and without crystal field splitting have already been presented in Ref. 29). In DMFT, non-local fluctuations are not included and thus do not affect the self-energy and spectral function. As a consequence, approaching the ordered states does not result in a pronounced temperature dependence of the DMFT spectra and self-energy.

A. SrO termination

Fig. 3 shows the DMFT Fermi surface for the SrO-terminated SrVO₃ monolayer at four different dopings (left to right). The upper panels display the contribution of the xy orbital and the lower panels the xz orbital (the yz orbital is equivalent to the latter if rotated by 90°).

We find the stoichiometric sample ($n = 1$) to be an orbitally polarized insulator⁴⁵ with a gap of about 1 eV, see Fig. 2. That is, the in-plane xy orbital is essentially half-filled, while the xz , yz orbitals are almost completely depleted. Hence, the undoped SrO-terminated SrVO₃ monolayer is an effective one-orbital system. The reduced orbital-degeneracy (with respect to the bulks threefold

t_{2g} orbitals) leads to a smaller critical interaction for the Mott state^{93,94}. This turns the undoped SrVO₃ monolayer Mott insulating with strong antiferromagnetic (AF) fluctuations.

Doping with 10% electrons or holes, we obtain a metal, see the panels with $n = 0.9$ and $n = 1.1$, respectively, in Fig. 2 and Fig. 3. The xz and yz orbitals are now slightly filled, pushing the AF phase transition to lower T , see Fig. 1, while strong AF spin fluctuations persist. The \mathbf{k} -integrated spectral function in Fig. 2 further shows that the xz and yz orbitals, while only slightly filled, already contribute a sizable amount to the quasi-particle peak at the Fermi level.

Similarities of this system to high- T_c cuprates are uncanny: While, here, the low-energy physics is dominated by a half-filled xy orbital instead of the $x^2 - y^2$ orbital in cuprates, we find a ratio of nearest to next-neighbor in-plane hopping $t'/t = +0.31$, ($t = -0.237$ eV, $t' = -0.073$ eV) which is essentially the same as found for YBa₂Cu₃O₇ and Bi₂Sr₂CaCu₂O₈⁹⁵, but t' has the opposite sign. In a one-band picture, one can compensate for the opposite sign by making a particle-hole transformation and we obtain an electron-like Fermi surface instead of a hole like one in cuprates. The decisive difference is however that, upon doping, the xz/yz orbitals become partially filled, leading to a different, multi-orbital kind of physics.

Indeed, at larger doping, $n = 1.5$, Fig. 1 indicates a checkerboard orbital-order (cOO) in DMFT with a spatially alternating occupation of the xz and yz orbitals, whereas the xy orbital does not participate in the cOO. Here, the xy and yz orbitals are already almost as much filled as the xz orbital as is evident from Fig. 2 and also from the Fermi surfaces in Fig. 3. As the xz (yz) lobes point in the $x-$ ($y-$) and z -direction, their Fermi surface in Fig. 3 is highly asymmetric, whereas their \mathbf{k} -integrated spectrum in Fig. 2 is similar to that of the xy orbital. In-between, around $n = 1.3$, the xz and yz orbitals are still significantly less filled, however the spectral function at the Fermi level $A(\omega = 0)$ is strongly enhanced, see Fig. 2. Ferromagnetic (FM) order therefore develops in Fig. 1 from the interplay of the Hund's coupling J and the hopping t ²⁹.

B. VO₂ termination

We now turn to the DMFT electronic structure of the VO₂-terminated surface. Again, we show Fermi surfaces (Fig. 5) and \mathbf{k} -integrated spectra (Fig. 4) for varying doping. For the VO₂- instead of the SrO-termination to the vacuum, the crystal-field splitting between the xz/yz and the xy orbital flips its sign²⁹. That is, the xy orbital now lies above the xz/yz orbitals. At $n = 1$, the latter accommodate all of the charge and their spectrum is split into upper and lower Hubbard bands, see Fig. 4, whereas the xy -orbital is unoccupied. The two degenerate xz and yz orbitals are at or near quarter filling around $n = 1$.

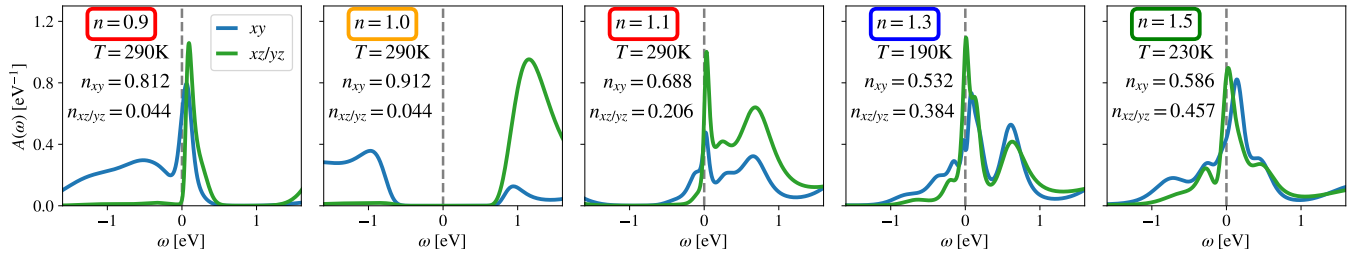


FIG. 2. **SrO-terminated monolayer** – DMFT spectral functions $A(\omega)$ for various fillings n and temperatures T : in the Mott insulating state ($n = 1.0$), in the vicinity of the AF ($n = 0.9, 1.1$), FM ($n = 1.3$) and cOO ($n = 1.5$) phases, resolved into orbital characters (xy and xz/yz). Colored boxes around fillings indicate the type of long-range orders realized at lower T , in correspondence to Fig. 1. At nominal filling ($n = 1$; orange) an orbitally polarized Mott insulator forms^{29,45}.

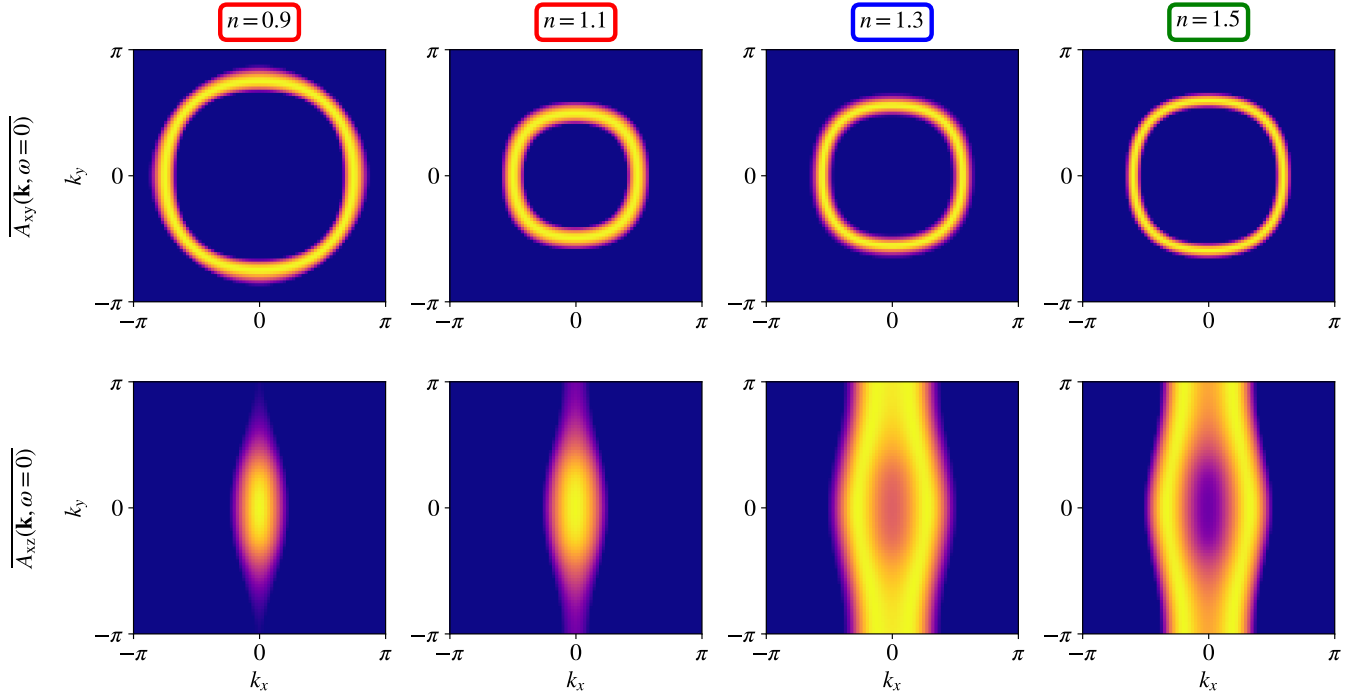


FIG. 3. **SrO-terminated monolayer** – DMFT Fermi surface for the points highlighted in Fig. 1a: $n = 0.9$ ($T = 290\text{K}$) and $n = 1.1$ ($T = 290\text{K}$) order AF at low T (red box indicating the color code of Fig. 1), FM at $n = 1.3$ ($T = 190\text{K}$; blue box), and cOO at $n = 1.5$ ($T = 230\text{K}$; green box).

This gives rise to checkerboard orbital fluctuations and, at low enough temperature, ordering (cOO) in DMFT, see Fig. 1. For slight hole doping and substantial electron doping, the cOO tendencies remain intact, but the SrVO₃ layer turns metallic. Inverting the role of the xz/yz and the xy orbitals compared to the SrO-termination, we now observe a small hole pocket for the xy orbital in Fig. 5, in agreement with their small filling in Fig. 4.

Reducing the filling from $n = 0.94$ to $n = 0.85$, this xy Fermi-surface pocket becomes slightly enhanced, albeit it remains small in Fig. 5. As for the fluctuations: because of their reduced filling, the xz/yz orbitals are no longer quarter-filled. Thus cOO gives way, first, to stripe orbital order (sOO) at $n = 0.85$ and, eventually, at lower fillings to FM, similar as for the two-band Hubbard model⁹⁶.

Further electron doping from $n = 1.23$ to $n = 1.3$ instead changes the DMFT ordered state from cOO to incommensurate magnetism (iM) with a small \mathbf{q} -vector in Fig. 1, see Ref. 29. It has, however, little effect on the spectral function and the Fermi surface in Fig. 4 and Fig. 5, respectively. The sharper Fermi surface for $n = 1.3$ can be explained by the slight decrease in the temperature and the fact that *local* DMFT correlations get reduced the farther we are away from half-filling, see Fig. 9 below.

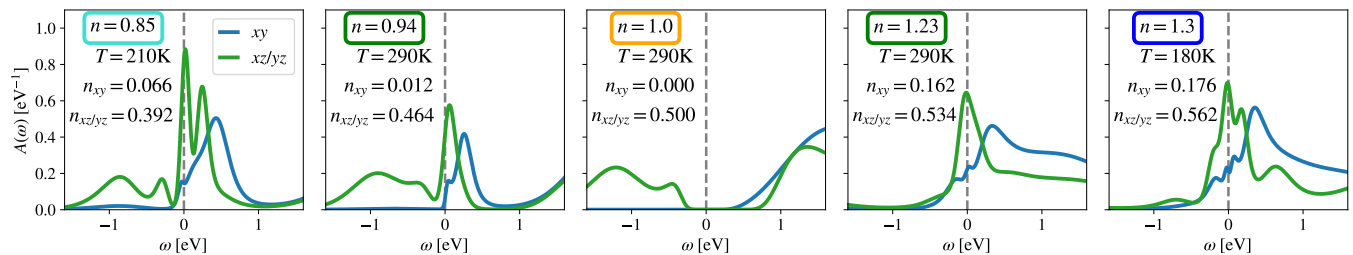


FIG. 4. **VO₂-terminated monolayer** – DMFT spectral functions $A(\omega)$ for various fillings n and temperature T : $n = 0.85$: sOO; $n = 0.94$: cOO; $n = 1.0$: Mott insulating cOO; $n = 1.23$: cOO; $n = 1.3$: iM. Otherwise identical to Fig. 2.

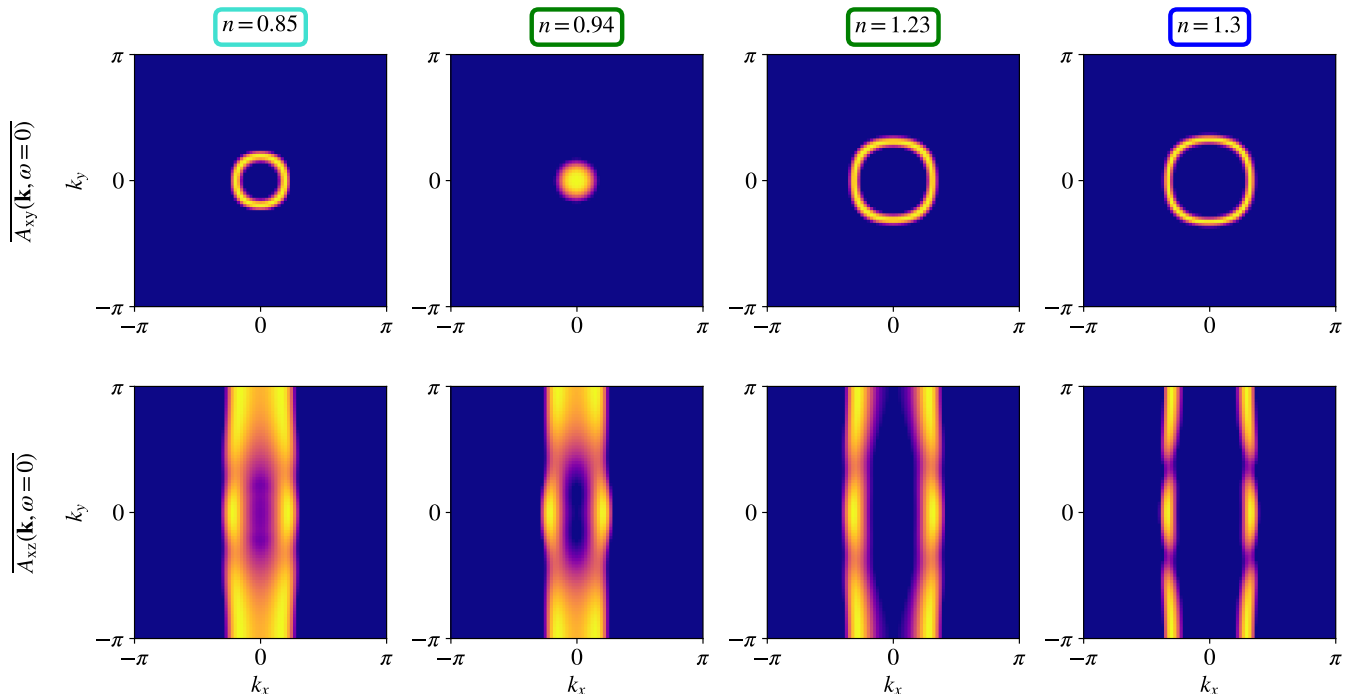


FIG. 5. **VO₂-terminated monolayer** – DMFT Fermi surface for the points highlighted in Fig. 1b: $n = 0.94$ ($T = 290$ K) and $n = 1.23$ ($T = 290$ K) order cOO at low T (green box indicating the color code of Fig. 1), $n = 0.85$ sOO ($T = 210$ K; turquoise box), and $n = 1.3$ iM ($T = 190$ K; blue box).

IV. DGA: MOMENTUM DIFFERENTIATION

On the dynamical mean-field level, many-body renormalizations are assumed to be isotropic (i.e., independent of momentum). In 3D this is mostly a good approximation (see, however, Ref. 97). Yet, when the effective dimensionality is reduced, as in our ultrathin film, renormalizations become increasingly non-local³⁰. The major question we will answer here is: *To what extent do the non-local critical fluctuations—in the vicinity of the associated ordered states—lead to momentum-selective renormalizations?* To elucidate this question, we use the AbinitioDGA^{54,69,70} methodology and scrutinize the electron self-energy $\Sigma(\mathbf{k}, i\nu)$ in the vicinity of the DMFT ordering instabilities summarized above.

A. SrO termination

Fig. 6 shows the real and imaginary part of the AbinitioDGA self-energy in the vicinity of the DMFT phase transitions where non-local correlations become strong. Shown are the two inequivalent orbitals, xy (top) and xz (middle panel) as a function of Matsubara frequency ν_n . The yz orbital is equivalent to the xz orbital if the momenta are rotated by 90° rotated; the DMFT self-energy is shown for comparison.

In the vicinity of half-filling, $n = 0.9$ and $n = 1.1$, AF spin fluctuations prevail with leading eigenvalue $\lambda_M(\pi, \pi) = 0.95$ and 0.79 , respectively, in the magnetic (M) channel at $\mathbf{q} = (\pi, \pi)$. Note, $\lambda = 1$ indicates a divergence of the susceptibility, i.e., an ordering instability. These AF spin fluctuations are driven by the xy orbital that is close to half filling, whereas the xz and yz or-

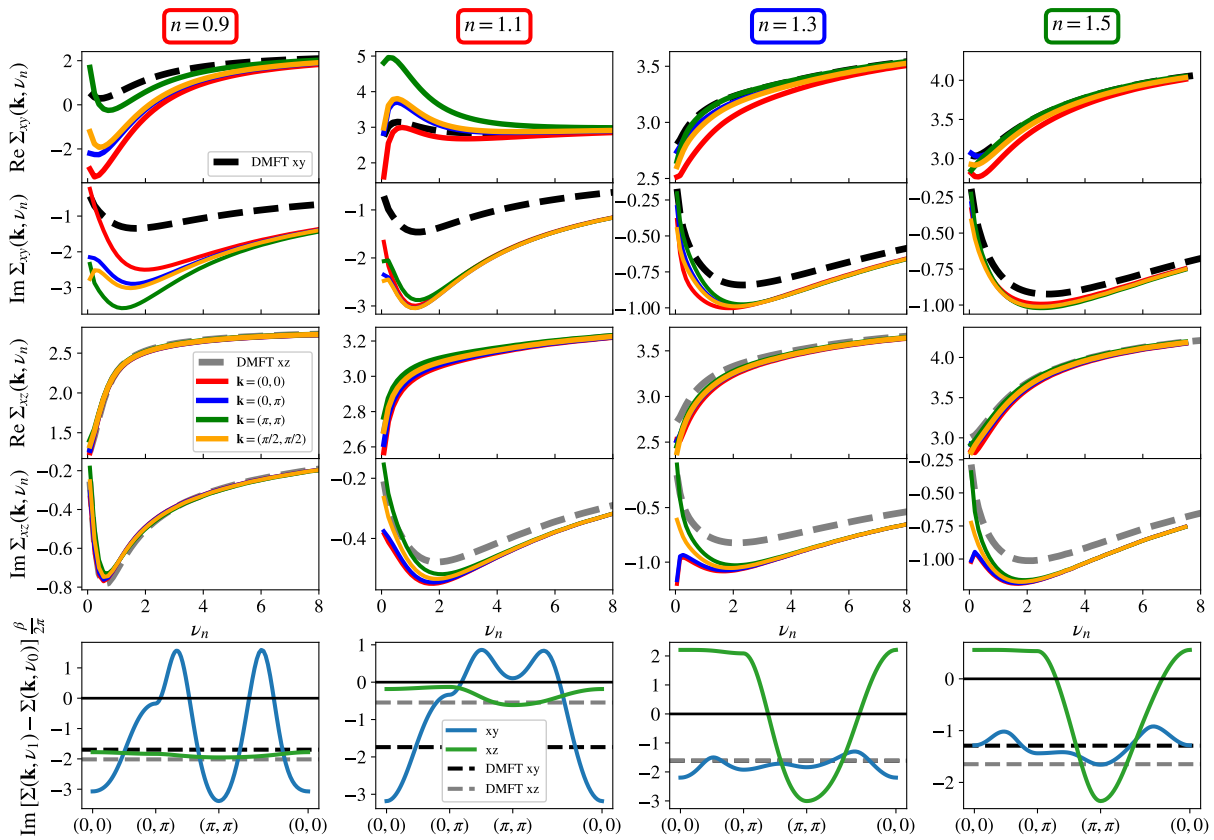


FIG. 6. **SrO-terminated monolayer – Momentum differentiation of the DGA self-energy.** Top 4 rows: real and imaginary parts for the xy and xz orbital at 4 different momenta, compared to DMFT, for the dopings and temperatures indicated in Fig. 1a. Bottom row: Slope of the imaginary part of the DGA self-energy for a path through the Brillouin zone. Negative values correspond to a Fermi-liquid like self-energy, positive values indicate the formation of a (pseudo)gap.

bitals rather act as passive bystanders²⁹. Consequently, we see for $n = 0.9$ and $n = 1.1$ in Fig. 6 a pronounced momentum differentiation only for the xy orbital.

The Matsubara frequency self-energy has the advantage that it does not require the ill-conditioned analytic continuation. Nonetheless, we can gain valuable information: The momentum differentiation of the real part of the self-energy in Fig. 6 between unoccupied [$\mathbf{k} = (0, 0)$, red] and occupied states [$\mathbf{k} = (\pi, \pi)$, green] signals that the quasi-particle poles at $\omega + \mu = \text{Re}\Sigma + \epsilon_{\mathbf{k}}$ are pushed further away from the Fermi energy, causing an overall *enhancement* of the bandwidth. The momentum differentiation between $\mathbf{k} = (0, \pi)$ (blue) and $\mathbf{k} = (\pi/2, \pi/2)$ (orange) that are closer to the Fermi level, indicates a deformation of the Fermi surface for $n = 0.9$, but not for $n = 1.1$ which has a similar self-energy for these two \mathbf{k} -points. Indeed a deformation is observed in Fig. 7, where the electron-like DMFT Fermi surface (Fig. 3) turns into a hole-like one in DGA for $n = 0.9$. For $n = 1.3$ with strong FM fluctuations ($\lambda_M(0, 0) = 0.78$) and $n = 1.5$ with strong cOO fluctuations in the density (D) channel ($\lambda_D(\pi, \pi) = 0.98$), the momentum differentiation of $\text{Re}\Sigma$ is less pronounced.

Let us now turn to $\text{Im}\Sigma$ from which we can read off

the scattering rate, as the $\nu_n \rightarrow 0$ -extrapolated value. Further, from its slope the quasi-particle renormalization $Z_{\mathbf{k}} = [1 - \partial \text{Im}\Sigma(\mathbf{k}, i\nu) / \partial \nu|_{\nu \rightarrow 0}]^{-1}$ is accessible for a Fermi liquid phase. A positive slope of $\text{Im}\Sigma(i\nu \rightarrow 0)$ indicates the crossover to a diverging (Mott-like) self-energy, which splits the spectrum and leads to an insulating gap.

Clearly, for all four fillings shown in Fig. 6, there are momenta for which the system exhibits non-Fermi liquid behavior, identifiable by a kink and a downturn in $\text{Im}\Sigma$ at low energies. In case of AF fluctuations ($n = 0.9$ and $n = 1.1$) this downturn is in the xy orbital, whereas it occurs in the xz (and yz) orbital which dominates the FM ($n = 1.3$) and cOO ($n = 1.5$) fluctuations. These kinks are salient indicators for the occurrence of a pseudogap state, and they get more pronounced when cooling the system toward the respective phase transition.

Interestingly, in the vicinity of the AF phase, the structure of the scattering rate is *opposite* to the cuprates: It is larger for the diagonal (π, π) direction than for the $(0, \pi)$ direction. This momentum differentiation on the Fermi surface is, however, much less pronounced than the momentum dependence perpendicular to the Fermi surface, i.e., comparing occupied vs. unoccupied states.

This can be seen in Fig. 6 (bottom), where we plot the

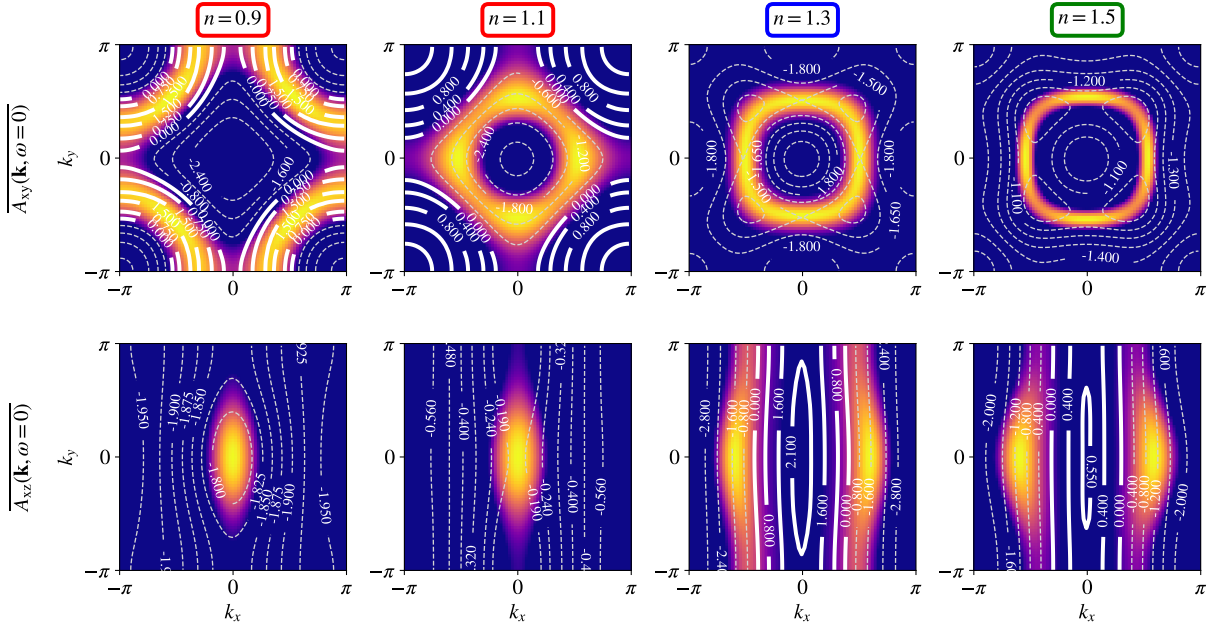


FIG. 7. **SrO-terminated monolayer – DGA Fermi surfaces** at the same dopings and T as in Fig. 3. The white contour lines represent isolines of the slope between the first two Matsubara frequencies of the imaginary part of Σ : Solid, fat lines indicate a *positive* slope, i.e., a kink in the self-energy, dashed, thin lines a *negative* value, suggestive of a Fermi-liquid-like state.

slope between the first two positive Matsubara frequencies, i.e., $slope = (\text{Im}\Sigma(i\nu_1) - \text{Im}\Sigma(i\nu_0))/\beta/(2\pi)$, along the indicated \mathbf{k} -path. Isolines of this slope are superimposed on the DGA Fermi surfaces in Fig. 7, with the sign indicated by solid, fat (positive) and dashed, thin (negative) lines. In the electron doped regime, the slope in $\text{Im}\Sigma$ is always negative on the Fermi surface, i.e., Fermi liquid-like. However, when moving away from the Fermi energy, we observe positive slopes, which corresponds to the kinks in Fig. 6: at $n = 1.1$ for the unoccupied xy states above the Fermi level; and at $n = 1.3$ and $n = 1.5$ for the occupied xz states. In the hole doped regime, at $n = 0.9$, we find $\text{Im}\Sigma$ isoline patterns similar to $n = 1.1$. However, owing to the larger xy -occupation in combination with the equally strong reconstruction through $\text{Re}\Sigma$, negative slopes of $\text{Im}\Sigma$ instead appear across the transformed xy Fermi surface. This insulating-like behavior is found only in the most relevant orbitals, i.e., the xy orbital for the AF fluctuations around $n = 1$, and the xz/yz orbitals where FM and cOO long-range fluctuations are dominant. The ancillary orbitals (xz/yz for $n = 1.1$ and xy for $n = 1.3, 1.5$) on the other hand exhibit only a comparatively minor momentum differentiation (see Fig. 6)—implying also a stark orbital differentiation.

B. VO₂ termination

The corresponding AbinitioDGA results for the VO₂-terminated SrVO₃ monolayer for the self-energy and the Fermi surface are presented in Fig. 8 and Fig. 9, respec-

tively. For cOO fluctuations at $n = 1.23$ ($\lambda_D(\pi, \pi) = 0.97$), the momentum differentiation of the self-energy and Fermi surface are qualitatively similar to the cOO results at $n = 1.5$ for the SrO-terminated layer. But for the cOO at $n = 0.94$ and sOO at $n = 0.85$, we only find a minor momentum differentiation of the self-energy, see Fig. 8. Correspondingly, the Fermi surface in Fig. 9 is similar to that of DMFT in Fig. 5, and there are no positive non-Fermi-liquid like slopes (solid lines in Fig. 9). This is surprising since the leading eigenvalue $\lambda_D(0, \pi) = \lambda_D(\pi, 0) = 0.985$ at $n = 0.85$ and $\lambda_D(\pi, \pi) = 0.91$ at $n = 0.94$ is similarly close to 1 as for $n = 1.23$ or the SrO-termination, indicating that strong orbital ordering fluctuations are present.

On the contrary, at $n = 1.3$, above iM order, we observe the by far strongest momentum differentiation in Fig. 8, even though $\lambda_M(\delta, \delta) = 0.97$ with $\delta \approx \pm\pi/4$ is again comparable to the strength of other fluctuations. A clear pole develops in the vicinity of the Fermi level not only for the xz and yz orbitals, that drive the iM ordering, but also for the xy orbital. This pole is so large that the spectrum splits into two parts, akin to the splitting into upper and lower Hubbard band; and it pushes the Fermi surface to $\mathbf{k} = (0, \pm\pi)$. However, the divergence occurs only for a region of the Brillouin zone that does not account for the Fermi surface of the respective orbital character.

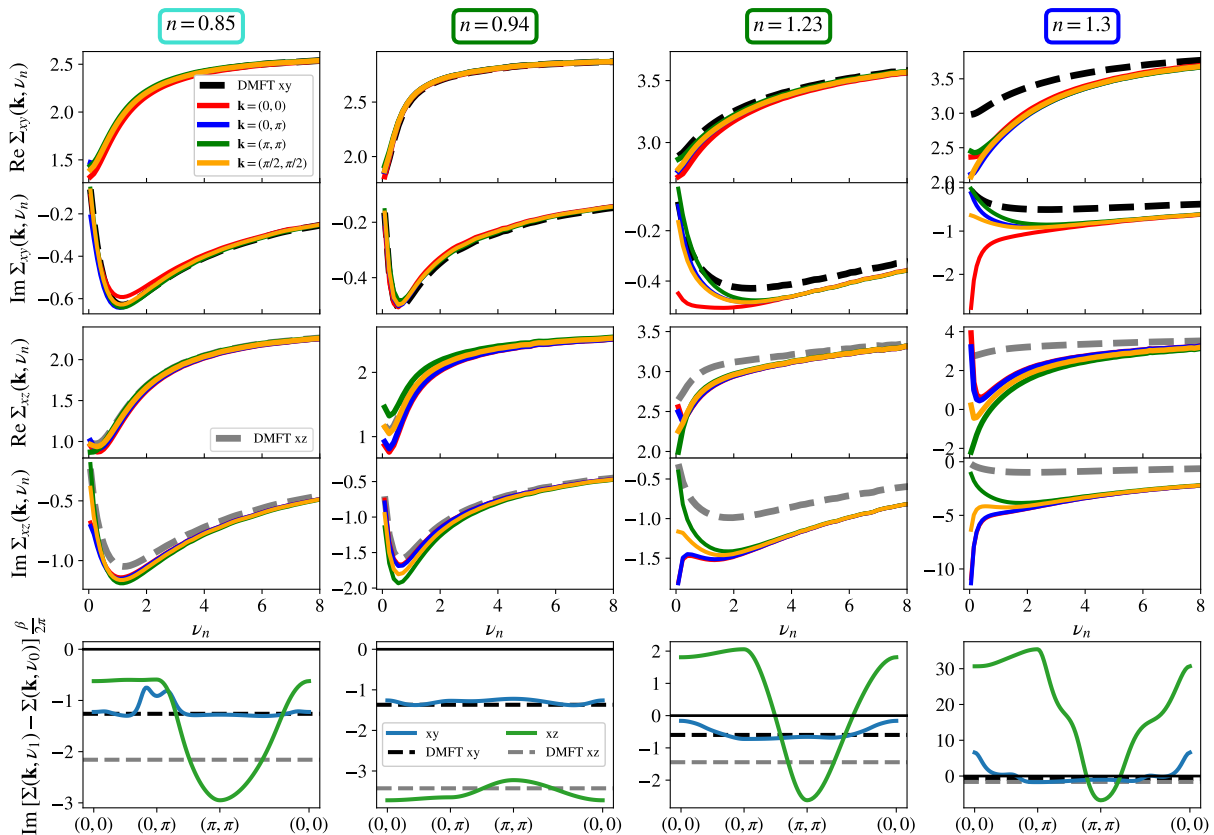


FIG. 8. **VO₂-terminated monolayer – momentum differentiation of the DGA self-energy.** Top 4 rows: real and imaginary parts for the xy and xz orbital for 4 different momenta (colors) and, for comparison, the DMFT self-energy (dashed) at the four dopings and T indicated by the “+” in Fig. 1b. Bottom row: Slope of the imaginary part of the DGA self-energy for a momentum path through the Brillouin zone.

V. DISCUSSION AND PERSPECTIVE

Recapitulating, we have studied a SrVO₃ monolayer on a SrTiO₃ substrate with two different surface terminations, SrO and VO₂, to vacuum within AbinitioDGA. Depending on the termination and filling, there are strong non-local fluctuations of various kinds: antiferromagnetic, ferromagnetic, incommensurate magnetic, striped or checkerboard orbital. These non-local fluctuations will suppress the mean-field DMFT ordering but also have pronounced effects on the self-energy—the focus of the present paper. They can deform the Fermi surface, as observed for antiferromagnetic ordering with $n = 0.9$ for SrO-terminated SrVO₃, and quite generally can lead to a strong enhancement of $\text{Im}\Sigma$. Strong non-local fluctuations can even cause the development of a pole in the self-energy, signaling the splitting of the spectrum into two parts—here not because of Mott-Hubbard physics but because of large non-local fluctuations. The latter is particularly strong for the incommensurate ferromagnetic phase of the VO₂-terminated SrVO₃ monolayer at $n = 1.3$ filling. First indications, i.e., downturns of the self-energy at the lowest Matsubara frequency are however ubiquitous for various dopings and both termina-

tions. While such non-local physics have been investigated quite intensively for antiferromagnetic fluctuations in the Hubbard model in the context of the cuprates, to the best of our knowledge it has not been analyzed before for orbital fluctuations.

The undoped ($n = 1$) SrVO₃ monolayer is Mott insulating and, for SrO-termination, appears to be akin to the cuprates with the xy orbital playing the role of the high- T_c ’s $x^2 - y^2$ orbital. However, electron-doping reveals the multi-orbital physics of the SrVO₃ system: The xy orbital is depopulated when adding electrons to the system, and all three orbitals, xy , xz and yz , participate in developing a quasi-particle resonance at the Fermi level.

For the cuprates, AF fluctuations lead to pseudogap physics with a momentum differentiation distinguishing between a Fermi liquid-like self-energy in the nodal direction on the Fermi surface, and a kink in the self-energy signaling the opening of a gap in the anti-nodal direction. Here, we also observe the joint presence of these two behaviors in the self-energy. However, the momentum differentiation is not realized *on* the Fermi surface but *perpendicular* to it: For the SrO-termination in the electron-doped regime, AF fluctuations lead to a Fermi liquid-like behavior for momenta on the occupied side

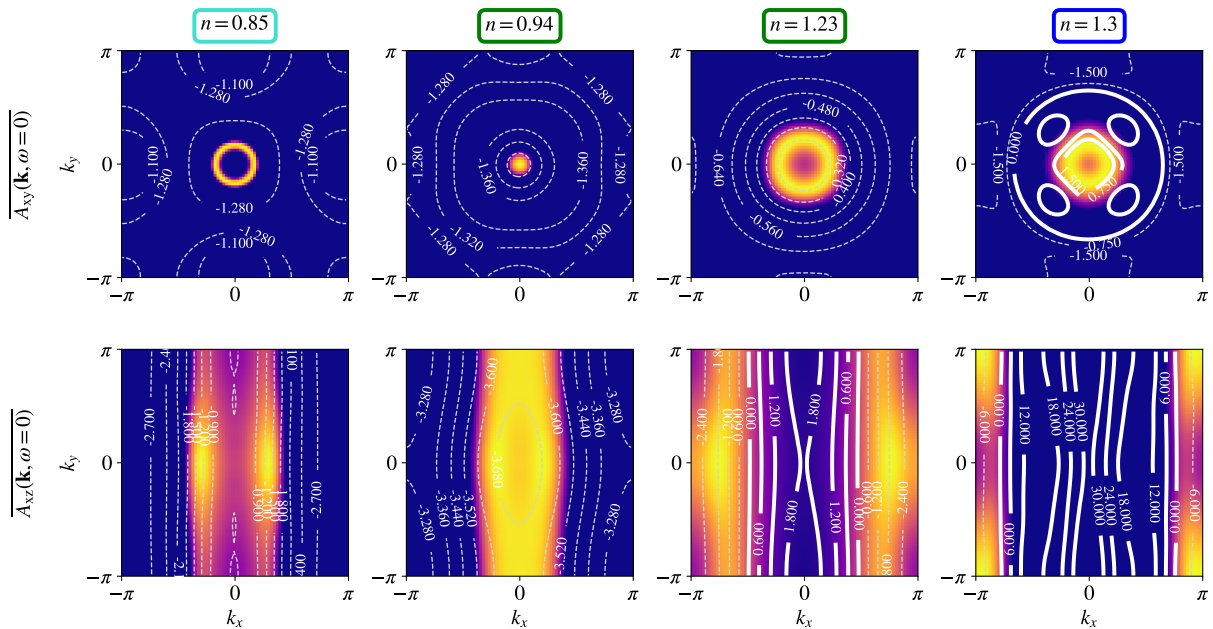


FIG. 9. **VO₂-terminated monolayer – DGA Fermi surfaces** at the same dopings and T as in Fig. 5. Isolines are again the low-energy slope of $\text{Im}\Sigma$, where the solid, fat lines represent a positive, and the dashed, thin lines represent a negative value.

of the Fermi surface (“ $k < k_F$ ”) and a kink-like insulating behavior in the imaginary part of the self-energy on the unoccupied side (“ $k > k_F$ ”). In case of FM and OO fluctuations, the momentum differentiation between occupied and unoccupied momenta is reversed.

For the VO₂ termination, iM fluctuations at $n = 1.3$ lead to massive non-local correlations and a pole in the self-energy. In contrast to all other cases not only the xz/yz orbitals—driving the iM fluctuations—are affected but also the ancillary xy orbital. Below half filling, on the other hand, cOO and sOO fluctuations only result in a minor momentum differentiation of the self-energy for the VO₂-terminated monolayer.

The imaginary part of the self-energy corresponds to the lifetimes and the broadening of the spectral function. Our results hence show that the lifetimes of an added hole or electron are extremely different. The hole-lifetime can be measured by angular resolved photoemission spectroscopy (ARPES); the electron lifetime by inverse photoemission spectroscopy, by ARPES at elevated temperatures, or in non-equilibrium situations (e.g., pump-probe measurements) in which states above the Fermi level become populated.

The differentiation between states above and below the Fermi surface that we observe is quite extreme. Technologically this might be exploited for thermoelectrics which rely on a strong electron-hole asymmetry^{98–101}. Particularly beneficial are sharp peaks in the spectral function on only one side of the Fermi level⁹⁸, as found for the SrO-terminated monolayer, see Fig. 3, within DMFT. There, *local* electronic correlations can enhance thermoelectricity through energy-dependent renormalizations that are different for electrons ($\omega < 0$) and holes

($\omega < 0$)^{99,102}. Our finding of a momentum-selectivity in the scattering rate may provide an *additional* route: A particle-hole asymmetry that is driven (or enhanced) by *non-local* renormalizations. Indeed, looking again at the SrO-terminated monolayer, OO and FM fluctuations at $n = 1.5$ and $n = 1.3$, respectively, drive a dispersive scattering rate¹⁰³ that is larger for occupied momenta (“ $k < k_F$ ”) then for empty states (“ $k > k_F$ ”): Specifically, the downward kinks in the xz -component of $\text{Im}\Sigma$, see Fig. 6, occur for $\mathbf{k} = (0, 0)$ and $\mathbf{k} = (0, \pi)$ which are inside the (DMFT) xz Fermi surface, see Fig. 3. For $\mathbf{k} = (\pi, \pi)$ and $\mathbf{k} = (\pi/2, \pi/2)$, which are outside the Fermi surface, the xz scattering rate instead decreases when approaching zero frequency. This electron-hole asymmetry of the scattering time will make the already electron-like DMFT thermopower even more negative, thus increasing its magnitude.

VI. CONCLUSIONS

Based on simulations of oxide ultrathin films, we demonstrated that, in (quasi-) two-dimensional systems, strong long-range fluctuations are quite generically reflected in a momentum differentiation of the self-energy, irrespective of the dominant fluctuation channel (spin/charge/orbital). Further, we demonstrated that this momentum differentiation has a much richer structure than the current focus on cuprates and pseudogap physics suggests: Strong variations in renormalizations may not only occur on the Fermi surface but also perpendicular to it. Our results call for a (re)examining—with beyond-DMFT methods—of correlated electron systems

that host strong non-local fluctuations: layered materials as well as ultra-thin oxide films and heterostructures.

ACKNOWLEDGMENTS

We thank M. Fuchs, A. Galler, J. Kaufmann, G. San-giovanni, P. Thunström and Z. Zhong for fruitful discussions. The authors acknowledge support from the Austrian Science Fund (FWF) through grants P 30819, P 32044, and P 30213. Calculations were performed on the Vienna Scientific Cluster (VSC).

* matthias.pickem@gmail.com

- ¹ Y. M. Vilks and A.-M. S. Tremblay, *J. Phys. I France* **7**, 1309 (1997).
- ² G. Rohringer, A. Toschi, A. Katanin, and K. Held, *Phys. Rev. Lett.* **107**, 256402 (2011).
- ³ G. Rohringer and A. Toschi, *Phys. Rev. B* **94**, 125144 (2016).
- ⁴ M. R. Norman, H. Ding, M. Randeria, J. C. Campuzano, T. Yokoya, T. Takeuchi, T. Takahashi, T. Mochiku, K. Kadowaki, P. Guptasarma, and D. G. Hinks, *Nature* **392**, 157 (1998).
- ⁵ T. Timusk and B. Statt, *Reports on Progress in Physics* **62**, 61 (1999).
- ⁶ M. R. Norman, D. Pines, and C. Kallin, *Advances in Physics* **54**, 715 (2005).
- ⁷ B. Keimer, S. A. Kivelson, M. R. Norman, S. Uchida, and J. Zaanen, *Nature* **518**, 179 (2015).
- ⁸ A. P. Kampf and J. R. Schrieffer, *Phys. Rev. B* **42**, 7967 (1990).
- ⁹ Y. M. Vilks and A.-M. S. Tremblay, *Europhysics Letters (EPL)* **33**, 159 (1996).
- ¹⁰ D. Rost, E. V. Gorelik, F. Assaad, and N. Blümer, *Phys. Rev. B* **86**, 155109 (2012).
- ¹¹ B. Kyung, V. Hankevych, A.-M. Daré, and A.-M. S. Tremblay, *Phys. Rev. Lett.* **93**, 147004 (2004).
- ¹² E. Gull, O. Parcollet, and A. J. Millis, *Phys. Rev. Lett.* **110**, 216405 (2013).
- ¹³ O. Cyr-Choinière, R. Daou, F. Laliberté, C. Collignon, S. Badoux, D. LeBoeuf, J. Chang, B. J. Ramshaw, D. A. Bonn, W. N. Hardy, R. Liang, J.-Q. Yan, J.-G. Cheng, J.-S. Zhou, J. B. Goodenough, S. Pyon, T. Takayama, H. Takagi, N. Doiron-Leyraud, and L. Taillefer, *Phys. Rev. B* **97**, 064502 (2018).
- ¹⁴ A. Kampf and J. R. Schrieffer, *Phys. Rev. B* **41**, 6399 (1990).
- ¹⁵ P. Monthoux and D. Pines, *Phys. Rev. B* **47**, 6069 (1993).
- ¹⁶ A. Abanov, A. V. Chubukov, and J. Schmalian, *Advances in Physics* **52**, 119 (2003).
- ¹⁷ Y. M. Vilks, *Phys. Rev. B* **55**, 3870 (1997).
- ¹⁸ W. Wu, M. S. Scheurer, M. Ferrero, and A. Georges, *Phys. Rev. Research* **2**, 033067 (2020).
- ¹⁹ J. González, F. Guinea, and M. A. H. Vozmediano, *Phys. Rev. Lett.* **84**, 4930 (2000).
- ²⁰ C. J. Halboth and W. Metzner, *Phys. Rev. Lett.* **85**, 5162 (2000).
- ²¹ C. Honerkamp and M. Salmhofer, *Phys. Rev. Lett.* **87**, 187004 (2001).
- ²² W. Wu, M. S. Scheurer, M. Ferrero, and A. Georges, *Phys. Rev. Research* **2**, 033067 (2020).
- ²³ F. Krien, P. Worm, P. Chalupa, A. Toschi, and K. Held, *arXiv:2107.06529* (2021).
- ²⁴ D. Fay, O. Loesener, and J. Appel, *Phys. Rev. B* **37**, 3299 (1988).
- ²⁵ P. Monthoux, *Phys. Rev. B* **68**, 064408 (2003).
- ²⁶ V. Hankevych, B. Kyung, and A.-M. S. Tremblay, *Phys. Rev. B* **68**, 214405 (2003).
- ²⁷ A. A. Katanin, A. P. Kampf, and V. Y. Irkhin, *Phys. Rev. B* **71**, 085105 (2005).
- ²⁸ A. A. Katanin, *Phys. Rev. B* **72**, 035111 (2005).
- ²⁹ M. Pickem, J. Kaufmann, K. Held, and J. M. Tomczak, *Phys. Rev. B* **104**, 024307 (2021).
- ³⁰ B. Klebel-Knobloch, T. Schäfer, A. Toschi, and J. M. Tomczak, *Phys. Rev. B* **103**, 045121 (2021).
- ³¹ Y.-M. Xu, P. Richard, K. Nakayama, T. Kawahara, Y. Sekiba, T. Qian, M. Neupane, S. Souma, T. Sato, T. Takahashi, H.-Q. Luo, H.-H. Wen, G.-F. Chen, N.-L. Wang, Z. Wang, Z. Fang, X. Dai, and H. Ding, *Nature Communications* **2**, 392 (2011).
- ³² S. J. Moon, A. A. Schafgans, S. Kasahara, T. Shibauchi, T. Terashima, Y. Matsuda, M. A. Tanatar, R. Prozorov, A. Thaler, P. C. Canfield, A. S. Sefat, D. Mandrus, and D. N. Basov, *Phys. Rev. Lett.* **109**, 027006 (2012).
- ³³ X. Zhou, P. Cai, A. Wang, W. Ruan, C. Ye, X. Chen, Y. You, Z.-Y. Weng, and Y. Wang, *Phys. Rev. Lett.* **109**, 037002 (2012).
- ³⁴ T. Shimojima, T. Sonobe, W. Malaeb, K. Shinada, A. Chainani, S. Shin, T. Yoshida, S. Ideta, A. Fujimori, H. Kumigashira, K. Ono, Y. Nakashima, H. Anzai, M. Arita, A. Ino, H. Namatame, M. Taniguchi, M. Nakajima, S. Uchida, Y. Tomioka, T. Ito, K. Kihou, C. H. Lee, A. Iyo, H. Eisaki, K. Ohgushi, S. Kasahara, T. Terashima, H. Ikeda, T. Shibauchi, Y. Matsuda, and K. Ishizaka, *Phys. Rev. B* **89**, 045101 (2014).
- ³⁵ P.-H. Lin, Y. Texier, A. Taleb-Ibrahimi, P. Le Fèvre, F. Bertran, E. Giannini, M. Grioni, and V. Brouet, *Phys. Rev. Lett.* **111**, 217002 (2013).
- ³⁶ M. Uchida, K. Ishizaka, P. Hansmann, Y. Kaneko, Y. Ishida, X. Yang, R. Kumai, A. Toschi, Y. Onose, R. Arita, K. Held, O. K. Andersen, S. Shin, and Y. Tokura, *Phys. Rev. Lett.* **106**, 027001 (2011).
- ³⁷ Y. K. Kim, O. Krupin, J. D. Denlinger, A. Bostwick, E. Rotenberg, Q. Zhao, J. F. Mitchell, J. W. Allen, and B. J. Kim, *Science* **345**, 187 (2014).
- ³⁸ I. H. Inoue, O. Goto, H. Makino, N. E. Hussey, and M. Ishikawa, *Phys. Rev. B* **58**, 4372 (1998).
- ³⁹ S.-K. Mo, J. D. Denlinger, H.-D. Kim, J.-H. Park, J. W. Allen, A. Sekiyama, A. Yamasaki, K. Kadono, S. Suga, Y. Saitoh, T. Muro, P. Metcalf, G. Keller, K. Held, V. Eyert, V. I. Anisimov, and D. Vollhardt, *Phys. Rev. Lett.* **90**, 186403 (2003).
- ⁴⁰ I. A. Nekrasov, K. Held, G. Keller, D. E. Kondakov, T. Pruschke, M. Kollar, O. K. Andersen, V. I. Anisimov, and

- D. Vollhardt, *Phys. Rev. B* **73**, 155112 (2006).
- ⁴¹ K. Byczuk, M. Kollar, K. Held, Y. F. Yang, I. A. Nekrasov, T. Pruschke, and D. Vollhardt, *Nat. Phys.* **3**, 168 (2007).
- ⁴² K. Held, R. Peters, and A. Toschi, *Phys. Rev. Lett.* **110**, 246402 (2013).
- ⁴³ K. Yoshimatsu, T. Okabe, H. Kumigashira, S. Okamoto, S. Aizaki, A. Fujimori, and M. Oshima, *Phys. Rev. Lett.* **104**, 147601 (2010).
- ⁴⁴ M. Kobayashi, K. Yoshimatsu, T. Mitsuhashi, M. Kitamura, E. Sakai, R. Yukawa, M. Minohara, A. Fujimori, K. Horiba, and H. Kumigashira, *Scientific Reports* **7**, 16621 (2017).
- ⁴⁵ Z. Zhong, M. Wallerberger, J. M. Tomczak, C. Taranto, N. Parragh, A. Toschi, G. Sangiovanni, and K. Held, *Phys. Rev. Lett.* **114**, 246401 (2015).
- ⁴⁶ M. Gu, S. Wolf, and J. Lu, *Advanced Materials Interfaces* **1** (2014), 10.1002/admi.201300126.
- ⁴⁷ Y. Okada, S.-Y. Shiau, T.-R. Chang, G. Chang, M. Kobayashi, R. Shimizu, H.-T. Jeng, S. Shiraki, H. Kumigashira, A. Bansil, H. Lin, and T. Hitosugi, *Phys. Rev. Lett.* **119**, 086801 (2017).
- ⁴⁸ J. Gabel, M. Pickem, P. Scheiderer, L. Dudy, B. Leikert, M. Fuchs, M. Stübinger, M. Schmitt, J. Küspert, G. Sangiovanni, J. M. Tomczak, K. Held, T.-L. Lee, R. Claessen, and M. Sing, *Advanced Electronic Materials* **n/a**, 2101006 (2021).
- ⁴⁹ W. Metzner and D. Vollhardt, *Phys. Rev. Lett.* **62**, 324 (1989).
- ⁵⁰ A. Georges and G. Kotliar, *Phys. Rev. B* **45**, 6479 (1992).
- ⁵¹ A. Georges, G. Kotliar, W. Krauth, and M. J. Rozenberg, *Rev. Mod. Phys.* **68**, 13 (1996).
- ⁵² A. Toschi, A. A. Katanin, and K. Held, *Phys. Rev. B* **75**, 045118 (2007).
- ⁵³ A. A. Katanin, A. Toschi, and K. Held, *Phys. Rev. B* **80**, 075104 (2009).
- ⁵⁴ A. Galler, P. Thunström, P. Gunacker, J. M. Tomczak, and K. Held, *Phys. Rev. B* **95**, 115107 (2017).
- ⁵⁵ G. Rohringer, H. Hafermann, A. Toschi, A. A. Katanin, A. E. Antipov, M. I. Katsnelson, A. I. Lichtenstein, A. N. Rubtsov, and K. Held, *Rev. Mod. Phys.* **90**, 025003 (2018).
- ⁵⁶ R. W. Godby, M. Schlüter, and L. J. Sham, *Phys. Rev. B* **37**, 10159 (1988).
- ⁵⁷ T. Miyake, C. Martins, R. Sakuma, and F. Aryasetiawan, *Phys. Rev. B* **87**, 115110 (2013).
- ⁵⁸ J. M. Tomczak, M. Casula, T. Miyake, and S. Biermann, *Phys. Rev. B* **90**, 165138 (2014).
- ⁵⁹ P. Blaha, K. Schwarz, G.-K.-H. Madsen, D. Kvasnicka, and J. Luitz, *Vienna University of Technology, Austria* (2001), ISBN 3-9501031-1-2.
- ⁶⁰ P. Blaha, K. Schwarz, F. Tran, R. Laskowski, G. K. H. Madsen, and L. D. Marks, *The Journal of Chemical Physics* **152**, 074101 (2020).
- ⁶¹ J. P. Perdew, K. Burke, and M. Ernzerhof, *Phys. Rev. Lett.* **77**, 3865 (1996).
- ⁶² C. Wang, H. Zhang, K. Deepak, C. Chen, A. Fouchet, J. Duan, D. Hilliard, U. Kentsch, D. Chen, M. Zeng, X. Gao, Y.-J. Zeng, M. Helm, W. Prellier, and S. Zhou, *Phys. Rev. Materials* **3**, 115001 (2019).
- ⁶³ J. Kunes, R. Arita, P. Wissgott, A. Toschi, H. Ikeda, and K. Held, *Computer Physics Communications* **181**, 1888 (2010).
- ⁶⁴ A. A. Mostofi, J. R. Yates, Y.-S. Lee, I. Souza, D. Vanderbilt, and N. Marzari, *Computer Physics Communications* **178**, 685 (2008).
- ⁶⁵ K. Held, *Advances in Physics* **56**, 829 (2007).
- ⁶⁶ J. Kaufmann, *github.com/josefkaufmann/ana_cont* (2019).
- ⁶⁷ J. Kaufmann and K. Held, (2021), arXiv:2105.11211 [cond-mat.str-el].
- ⁶⁸ J. M. Tomczak, P. Liu, A. Toschi, G. Kresse, and K. Held, *The European Physical Journal Special Topics* **226**, 2565 (2017).
- ⁶⁹ A. Galler, J. Kaufmann, P. Gunacker, M. Pickem, P. Thunström, J. M. Tomczak, and K. Held, *Journal of the Physical Society of Japan* **87**, 041004 (2018).
- ⁷⁰ A. Galler, P. Thunström, J. Kaufmann, M. Pickem, J. M. Tomczak, and K. Held, *Computer Physics Communications* **245**, 106847 (2019).
- ⁷¹ H. Kusunose, *J. Phys. Soc. Jpn.* **75**, 054713 (2006).
- ⁷² A. N. Rubtsov, M. I. Katsnelson, and A. I. Lichtenstein, *Phys. Rev. B* **77**, 033101 (2008).
- ⁷³ G. Rohringer, A. Toschi, H. Hafermann, K. Held, V. I. Anisimov, and A. A. Katanin, *Phys. Rev. B* **88**, 115112 (2013).
- ⁷⁴ C. Taranto, S. Andergassen, J. Bauer, K. Held, A. Katanin, W. Metzner, G. Rohringer, and A. Toschi, *Phys. Rev. Lett.* **112**, 196402 (2014).
- ⁷⁵ G. Li, *Phys. Rev. B* **91**, 165134 (2015).
- ⁷⁶ O. Parcollet, M. Ferrero, T. Ayrál, H. Hafermann, I. Krivenko, L. Messio, and P. Seth, *Computer Physics Communications* **196**, 398 (2015).
- ⁷⁷ G. Sordi, K. Haule, and A.-M. S. Tremblay, *Phys. Rev. B* **84**, 075161 (2011).
- ⁷⁸ S. Sakai, G. Sangiovanni, M. Civelli, Y. Motome, K. Held, and M. Imada, *Phys. Rev. B* **85**, 035102 (2012).
- ⁷⁹ T. Schäfer, A. Toschi, and K. Held, *Journal of Magnetism and Magnetic Materials* **400**, 107 (2016).
- ⁸⁰ T. Schäfer, F. Geles, D. Rost, G. Rohringer, E. Arrigoni, K. Held, N. Blümer, M. Aichhorn, and A. Toschi, *Phys. Rev. B* **91**, 125109 (2015).
- ⁸¹ O. Gunnarsson, T. Schäfer, J. P. F. LeBlanc, E. Gull, J. Merino, G. Sangiovanni, G. Rohringer, and A. Toschi, *Phys. Rev. Lett.* **114**, 236402 (2015).
- ⁸² J. Gukelberger, E. Kozik, and H. Hafermann, *Phys. Rev. B* **96**, 035152 (2017).
- ⁸³ T. Schäfer, N. Wentzell, F. Šimkovic, Y.-Y. He, C. Hille, M. Klett, C. J. Eckhardt, B. Arzhang, V. Harkov, F. m. c.-M. Le Régent, A. Kirsch, Y. Wang, A. J. Kim, E. Kozik, E. A. Stepanov, A. Kauch, S. Andergassen, P. Hansmann, D. Rohe, Y. M. Vilck, J. P. F. LeBlanc, S. Zhang, A.-M. S. Tremblay, M. Ferrero, O. Parcollet, and A. Georges, *Phys. Rev. X* **11**, 011058 (2021).
- ⁸⁴ A. E. Antipov, E. Gull, and S. Kirchner, *Phys. Rev. Lett.* **112**, 226401 (2014).
- ⁸⁵ T. Schäfer, A. A. Katanin, K. Held, and A. Toschi, *Phys. Rev. Lett.* **119**, 046402 (2017).
- ⁸⁶ T. Schäfer, A. A. Katanin, M. Kitatani, A. Toschi, and K. Held, *Phys. Rev. Lett.* **122**, 227201 (2019).
- ⁸⁷ P. Werner, A. Comanac, L. de' Medici, M. Troyer, and A. J. Millis, *Phys. Rev. Lett.* **97**, 076405 (2006).
- ⁸⁸ E. Gull, A. J. Millis, A. I. Lichtenstein, A. N. Rubtsov, M. Troyer, and P. Werner, *Rev. Mod. Phys.* **83**, 349 (2011).
- ⁸⁹ M. Wallerberger, A. Hausoel, P. Gunacker, A. Kowalski, N. Parragh, F. Goth, K. Held, and G. Sangiovanni, *Com-*

- puter Physics Communications **235**, 388 (2019).
- ⁹⁰ P. Gunacker, M. Wallerberger, E. Gull, A. Hausoel, G. Sangiovanni, and K. Held, Phys. Rev. B **92**, 155102 (2015).
- ⁹¹ J. Kaufmann, C. Eckhardt, M. Pickem, M. Kitatani, A. Kauch, and K. Held, Phys. Rev. B **103**, 035120 (2021).
- ⁹² Due to the multi-orbital nature and the temperature scaling of the DGA we are restricted in temperature, i.e. we are not able to approach the FM instability much further.
- ⁹³ O. Gunnarsson, E. Koch, and R. M. Martin, Phys. Rev. B **54**, R11026 (1996).
- ⁹⁴ E. Pavarini, S. Biermann, A. Poteryaev, A. I. Lichtenstein, A. Georges, and O. K. Andersen, Phys. Rev. Lett. **92**, 176403 (2004).
- ⁹⁵ E. Pavarini, I. Dasgupta, T. Saha-Dasgupta, O. Jepsen, and O. K. Andersen, Phys. Rev. Lett. **87**, 047003 (2001).
- ⁹⁶ K. Held and D. Vollhardt, The European Physical Journal B - Condensed Matter and Complex Systems **5**, 473 (1998).
- ⁹⁷ T. Schäfer, A. Toschi, and J. M. Tomczak, Phys. Rev. B **91**, 121107(R) (2015).
- ⁹⁸ G. Mahan and J. Sofo, Proc. Nat. Acad. Sci. USA **93**, 7436 (1996).
- ⁹⁹ K. Held, R. Arita, V. I. Anisimov, and K. Kuroki, in *Properties and Applications of Thermoelectric Materials*, NATO Science for Peace and Security Series B: Physics and Biophysics, edited by V. Zlatić and A. Hewson (Springer, 2009) p. 141.
- ¹⁰⁰ V. Zlatić and R. Monnier, *Modern Theory of Thermoelectricity* (Oxford University Press, 2014).
- ¹⁰¹ J. M. Tomczak, J. Phys.: Condens. Matter (Topical Review) **30**, 183001 (2018).
- ¹⁰² K. Haule and G. Kotliar, in *Properties and Applications of Thermoelectric Materials*, edited by V. Zlatić and A. C. Hewson (Springer Netherlands, Dordrecht, 2009) pp. 119–131.
- ¹⁰³ P. Sun, W. Xu, J. M. Tomczak, G. Kotliar, M. Søndergaard, B. B. Iversen, and F. Steglich, Phys. Rev. B **88**, 245203 (2013).